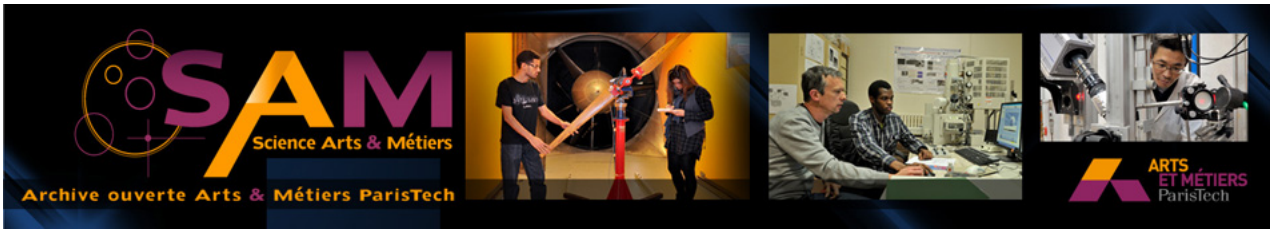

Tribological response of AA 2024-T3 aluminium alloy coated with a DLC duplex coating

M.H. Staia [a,b,d,*,1], E.S. Puchi Cabrera [a,c,d,2], A. Iost [b], A. Zairi [b], S. Belayer [e,3], A. Van Gorp [b]

[a] Escuela de Ingeniería Metalúrgica y Ciencia de los Materiales, Facultad de Ingeniería, Universidad Central de Venezuela, Los Chaguaramos, Caracas 1041, Venezuela
[b] Arts et Métiers ParisTech—Centre de Lille, 8, Boulevard Louis XIV, 59000 Lille Cedex, France
[c] Université Lille Nord de France, F-59000 Lille; USTL, LML, CNRS, UMR 8107, F-59650 Villeneuve d'Ascq, France
[d] Academia Nacional de Ingeniería y Hábitat, Palacio de las Academias, Dirección Postal 1723, Caracas 1010, Venezuela
[e] ENSCL (École Nationale Supérieure de Chimie de Lille) Laboratoire PERF (Procédés d'Élaboration des Revêtements Fonctionnels) LSPES—UMR/CNRS 8008, Villeneuve d'Ascq, France

A B S T R A C T

Considerable improvement in the tribological response was achieved during sliding wear tests against alumina ball, when AA 2024-T3-aluminium alloy substrate was coated with DLC/NiP duplex coating. Quantitative EPMA analysis carried out on the coated sample cross-section coupled with nanoindentation techniques allowed the identification of the coated system architecture as composed of 4 main layers, with distinct mechanical properties, on top of the aluminium substrate: DLC (a:C-H chromium dopped layer and graded layer of CrC), a newly formed graded layer of CNiPCr, product of the interdifusion during PVD processing, and the NiP coating. The change in the elastic modulus with penetration depth was described by means of an original approach that was developed for its specific application to multilayer coatings.

Keywords:
DLC coating
Nanoindentation
Electroless nickel
Elastic contact

1. Introduction

In the past few years the improvement of the wear and/or corrosion resistance properties of Al, Ti and Mg, as well as their alloys, has constituted an important scientific and technological objective for the surface engineering community, as a consequence of the increasing application of these materials in different industrial fields.

Amongst the surface engineering methods used to protect aluminium alloys, electroless deposition of NiP has drawn the attention for more than one decade [1]. Electroless is an effective technique for deposition of an uniform, crack free and adherent metallic coating to a substrate without applying an external electrical circuit and the results of many investigations related to the use of this type of coatings have shown considerable improvement of the coated systems performance [2–4].

Another favoured candidate is DLC, which in the past few years has been deposited on light alloys such as Mg, Ti and Al with the aim of enhancing their tribological behaviour, thus increasing their possibility of being used mainly in the aerospace, automotive and military industries, as well as in the manufacture of medical devices [5].

Nevertheless, it is also important to mention the various surface engineering processes such as nitriding, laser gas alloying, electron beam surface alloying and duplex surface engineering techniques that have been used for protection of aluminium and titanium components against wear [6].

However, as it is well known that, when a hard coating is deposited onto these materials, the existing difference between the mechanical properties of the substrate and coating could give rise to a low-carrying capacity of the substrate with the subsequent cracking of the coating. The deformation and fracture behaviour of these kinds of systems was recently demonstrated by means of FIB studies carried out by Xie et al. [7]. Therefore, extensive research work has been carried out with the aim of preventing these failures by decreasing the

* Corresponding author.
E-mail addresses: mhstaia@gmail.com (M.H. Staia), Eli.Puchi@univ-lille1.fr (E.S. Puchi Cabrera), alain.iost@ensam.eu (A. Iost), amal.zairi@gmail.com (A. Zairi), Severine.Bellayer@ensc-lille.fr (S. Belayer), adrien.vangorp@ensam.eu (A. Van Gorp).
[1] School of Metallurgy and Materials Science, Faculty of Engineering, Universidad Central de Venezuela, Caracas, Venezuela. Currently at: Arts et Métiers ParisTech—Centre de Lille, 8, Boulevard Louis XIV, 59000 Lille Cedex, France.
[2] School of Metallurgical Engineering and Materials Science, Faculty of Engineering, Universidad Central de Venezuela, Postal address 47885, Los Chaguaramos, Caracas, 1040, Venezuela. Currently at: Université Lille Nord de France, USTL, LML, CNRS, UMR 8107, F-59650 Villeneuve d'Ascq, France.
[3] ENSCL (École Nationale Supérieure de Chimie de Lille) Laboratoire PERF (Procédés d'Élaboration des Revêtements Fonctionnels) LSPES—UMR/CNRS 8008, France.

Young's modulus mismatch and/or yield stress difference between the film and substrate [8–12].

In the present research work, a detailed tribological characterization of three systems will be conducted, namely, the uncoated AA 2024-T3 aluminium alloy substrate, the substrate coated with electroless NiP and the substrate coated with a duplex system DLC/NiP.

For the first time, the discussion of the results will be coupled with an extensive mechanical and compositional characterization of the DLC/CrC/NiP/aluminium alloy system as a whole, in order to determine the changes produced during the PVD deposition process. The intrinsic hardness and elastic modulus of each individual layer in the multilayer system will be evaluated by means of the modified form of the model originally advanced by Jönsson and Hogmark [13], as proposed by Iost et al. [14] and by modifying the model advanced by Perriot and Barthel [15], in order to be applicable to multilayer coatings, respectively.

The information concerning the predicted change of elastic modulus with penetration depth will be employed in the computation of the change in von Mises stress with distance from the surface by means of the classical Hertzian formulation for this multilayer coated system, taking into consideration the compatibility of strains at each interface. This evaluation, proposed here for the first time, will provide information about the mechanical stability of the coated system under the experimental conditions during the sliding test.

2. Experimental

Bars of 19.5 mm in diameter of an AA 2024-T3 aluminium alloy were provided by Allusuisse, Switzerland. The alloy exhibited a yield stress, $R_{0.2}=450$ MPa. Samples of 5 mm thickness were cut and, subsequently, mirror polished ($R_a=0.04\pm0.01$ μm) by means of standard metallographic procedures. The NiP electroless was deposited industrially by Reliable Plating Inc. (USA). Subsequently, the NiP samples were polished to obtain a roughness of 0.2 ± 0.01 μm before the DLC deposition. The DLC film, commercially known as Dymon-iC TM (hydrogenated a-C:H), was deposited by Teer Coatings, U.K., by means of closed field unbalanced magnetron sputtering ion platting (CFUBMSIP), coupled with plasma assisted chemical vapour deposition (PACVD). Details of the deposition process have been described elsewhere [16].

The hardness and the elastic properties of the DLC coating have been determined by means of nanoindentation tests using a MTS XP Nano Indenter under a continuous stiffness measurement mode and equipped with a Berkovich indenter. Prior to indentation, the tip calibration was carried out on fused silica. 25 indentations were conducted on three different samples and the elastic modulus, E, and hardness, H, were recorded continuously versus the indentation depth, h, up to 7000 nm, at a constant indentation rate of 0.05 s^{-1}. The results were analyzed by means of the Oliver and Pharr method [17]. In this case, the NiP deposit could be considered as the "substrate" due to its large thickness of ~52 μm. Therefore, it is possible to determine the correct hardness values of both the DLC and CrC films by means of an appropriate hardness model, as shown in the forthcoming.

The adhesion tests of the DLC coating deposited on top of the electroless NiP was carried out by means of a commercial microscratch tester (Scratch Tester Millennium 200) fitted with a Rockwell spherical diamond indenter (tip radius of 200 μm) and equipped with an acoustic emission detector. The indenter loading rate was of 120 N/min and was it was applied to a 5 mm scratch length, allowing a maximum load of 60 N to be achieved. The load, at which the uncovered substrate will be visible regularly along the scratch track, has been considered as the critical adhesive load. The latter was determined from the response of the recorded parameters, coupled with the evaluation of the optical micrographs obtained from the microscope attached to the scratch tester. Additional analyses using a Cameca SX100 electron probe micro analyzer was performed to the last part of the scratch, for higher loads, in order to detect with precision the nature of the failures found for this coated system.

The friction and wear tests were run in a standard ball on disc tribometer using of 2 and 5 N, respectively, a sliding speed of 0.05 m/s and 800 m sliding distance. The tests were carried out in air with $55\pm5\%$ humidity. For comparison, the uncoated aluminium alloy samples were also tested in the same conditions. The morphological characterization of all wear scars obtained from the tribological tests for all three systems under study was conducted by means of SEM techniques, which allowed the determination of the wear mechanism. A Cameca SX100 electron probe micro analyser (EPMA) with four wavelength dispersive X-ray spectrometers (WDS) was used to perform microscopic and elemental analyses within the wear tracks. Back scattered electrons (BSE) images were carried out at 20 kV, 20 nA. Low and high magnification images were taken in various parts of the samples in order to have representative images of the samples. Both X-ray mappings and profiles of chromium (Cr), nickel (Ni), phosphorous (P) and carbon (C) were carried out at 15 kV, 40 nA. A PC2 crystal was used to detect the O and C $K\alpha$ X-rays, a PET crystal for the Ar, P and Cr $K\alpha$ X-rays, a LiF crystal for the Ni $K\alpha$ X-rays and

Roughness measurements and the wear track profiles were determined by means of a Veeco Wyko NT9300 profilometer. The cross section area was computed by the numerical integration of the curve corresponding to the interpolated function between each experimental depth data point, employing a cubic spline interpolation.

The registered profiles allowed the determination of the maximum coating penetration depth. Wear volumes were obtained by multiplying the cross-sectional wear track area by the length of the wear track. The specific wear rate k was obtained from the ratio between wear volume and the applied load per unit of sliding distance (m^3/N m).

3. Results and discussion

3.1. Coatings morphology and roughness

The NiP coating cross section, as well as its morphology, is shown in Fig. 1a and b, respectively. Additionally, profilometry measurements were carried out indicating that, in the as-received condition, the NiP has a roughness value $R_a=0.42\pm0.01$ μm (see Fig. 1c). As it can be observed, the coating deposited on top of the aluminium alloy has a uniform thickness of $\sim50\pm2$ μm. The morphology of the NiP coating is characteristic of these kinds of alloys, in which the existence of a typical growth is noticed. An amount of P of ~9.8%, as determined by means of fluorescence spectroscopy for the as-deposited coating, indicates the presence of an amorphous nickel-phosphorous phase classified as high phosphorous coating [1].

The morphology of the DLC coating (see Fig. 2a and b) shows the presence of the typical defects that are inherent to this PAPVD deposition process. A roughness of approximately 0.18 μm ± 0.01 was determined, which is very similar to that of the electroless NiP, whose surface was prepared before deposition. It is well known [5] that DLC films, being structurally amorphous, could closely mimic the original surface roughness of the substrate material. The overall coating thickness of the DLC (a-C:H+CrC) was determined by means of Calotest (CSEM, Switzerland) measurements and it was found to be of $\sim2.2\pm0.1$ μm.

Fig. 3 presents a micrograph corresponding to the fracture of the DLC coating on top of the NiP, indicating that near the interface PVD coating/NiP a less dense structure of the surface region is present. Also, various dark spots (pointed out by white arrows), corresponding to the Ar incorporation in the structure, can be

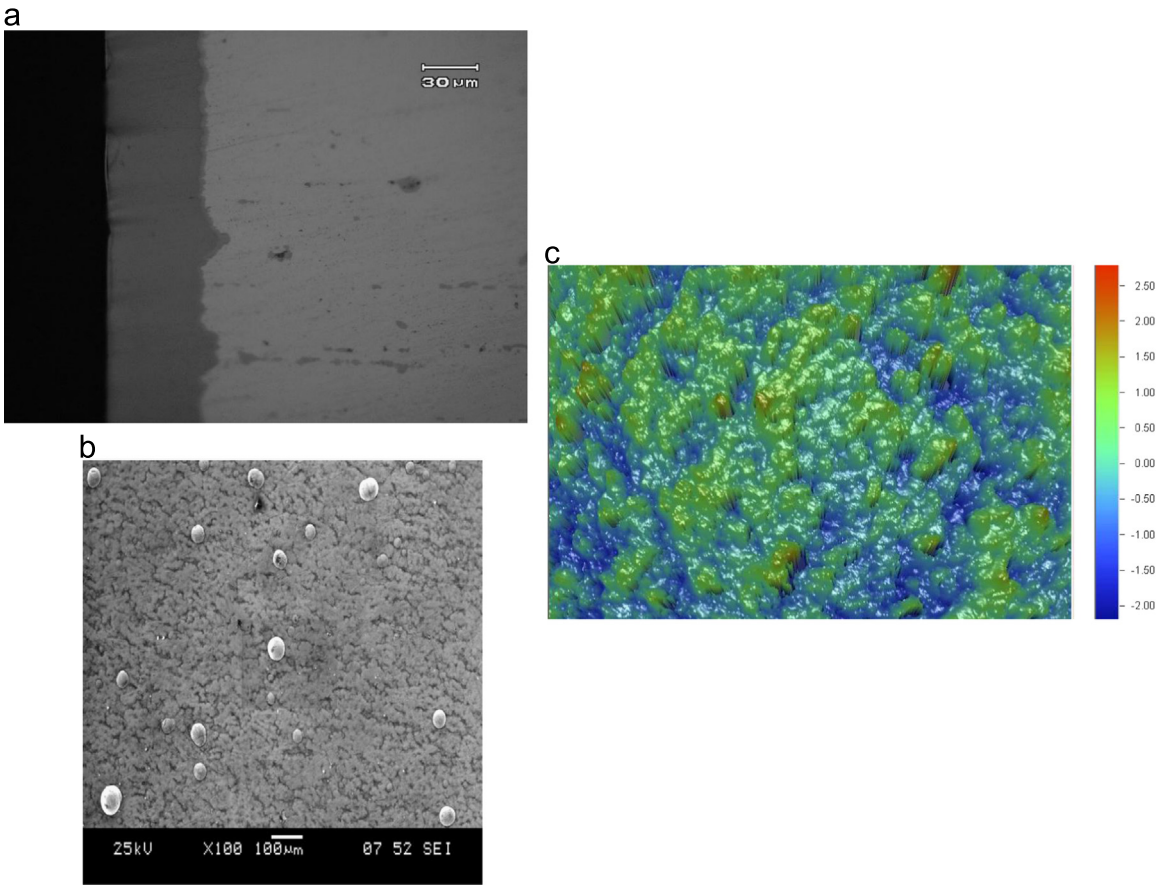

Fig. 1. Microstructural characteristics of the as-received electroless NiP coating: (a) coating cross section; (b) SEM micrograph showing the coating morphology; (c) 3D roughness profile of the coating surface.

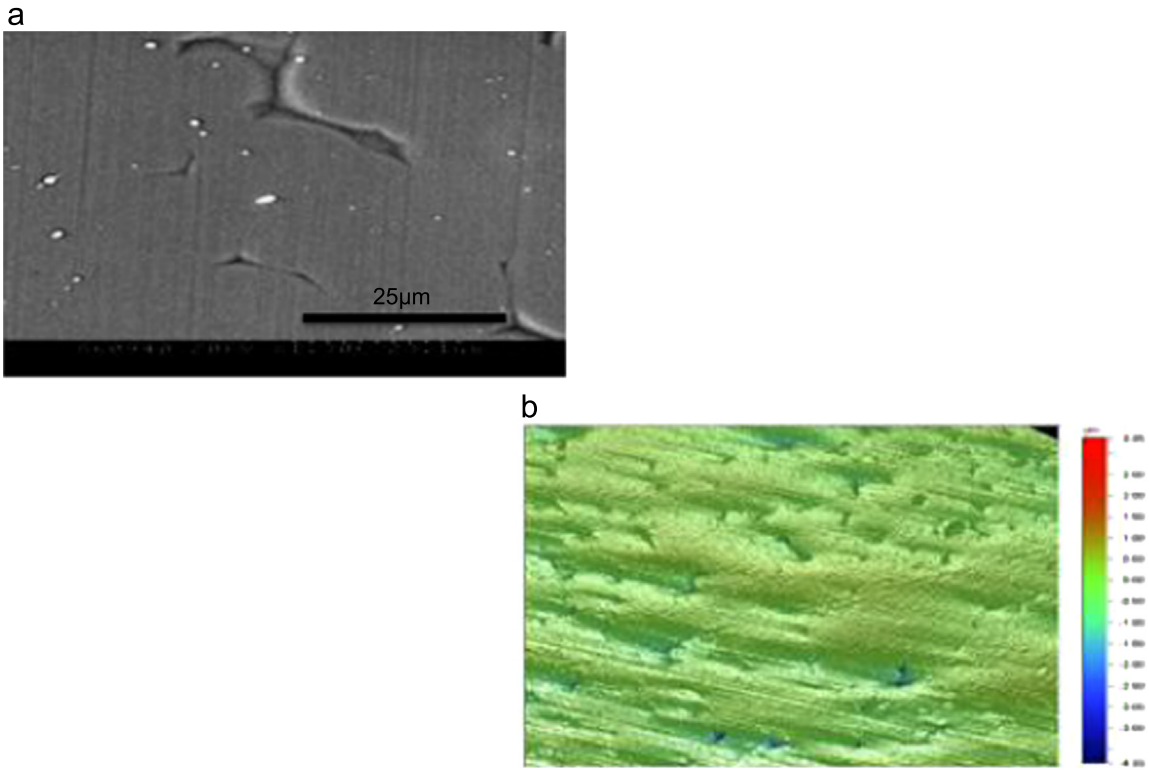

Fig. 2. (a) SEM micrograph of the DLC coating deposited on top of the electroless NiP coating; (b) 3D roughness profile of the coated surface.

observed. Now, it has to be remembered that in order to ensure a better adhesion, the surface of the NiP coating prior to DLC deposition was cleaned by ion bombardment with ionized Ar atoms from the glow discharge plasma. The ion cleaning could have been accompanied with an increase in the substrate temperature due to ion bombardment, as it has been indicated by Schönjahn et al. [18]. Also, it could have implied the presence of Ar gas inclusions in the material close to the interface region, which could have produced a considerable change in the appearance of the NiP microstructure.

As it has already been described [16], during the deposition procedure this cleaning process is followed by the deposition of a Cr film on top of the electroless NiP coating, using argon as the working gas. In turn, this is followed by a chromium carbide graded layer, which requires the addition of butane in the system and, finally, the a-C:H film is deposited.

Very coarse NiP grains are noticed, as shown in Fig. 3, which could mainly be attributed to the recrystallization process that probably took place at the temperature attained during the ion cleaning process, which was somewhat higher than that reported for the PVD coating deposition process [16].

Also, interdifusion between the PVD coating and the NiP coating was promoted during processing. This could be observed from the SEM micrograph and elements X-ray mapping, as well as from the quantitative elemental analysis carried out by means of electron probe micro analysis (EPMA) on the coated system cross section. Such an analysis started from the surface and was conducted up to approximately 125 μm inside the sample, towards the aluminium substrate. The results are presented in Fig. 4a and b

As can be observed from Fig. 4a, some argon and oxygen pick up took place during the DLC deposition, confirming the SEM morphology presented above in Fig. 3. However, it was difficult to determine with precision their concentration without the appropriate standards.

As shown in Fig. 5, the C content decreases from approximately 74 wt% at the surface, to about 8 wt% at a distance from the surface somewhat less than 4 μm, remaining at this constant value up to the NiP/Al alloy interface. Such a change in C content clearly indicates a diffusion process, which is restricted to just this short distance. The fact that the C composition profile is flat at larger distances is unlikely to be due to C diffusion, given small diffusivity of this element either in Ni and Al. On the contrary, the flat C profiles observed in the NiP deposit, as well as in the 2023-T3 aluminium alloy could just be a consequence of C pollution during sample preparation for its analysis by means of EPMA techniques. Therefore, the EPMA results, presented in Fig. 5 and summarized in Table 1, allow a quite precise determination of the variation of the elemental concentrations of Ni, P and Cr, that took place during PVD deposition between the PVD coating/NiP interface. However, in spite that it is clearly observed that a change in C content occurred, its precise composition cannot be determined.

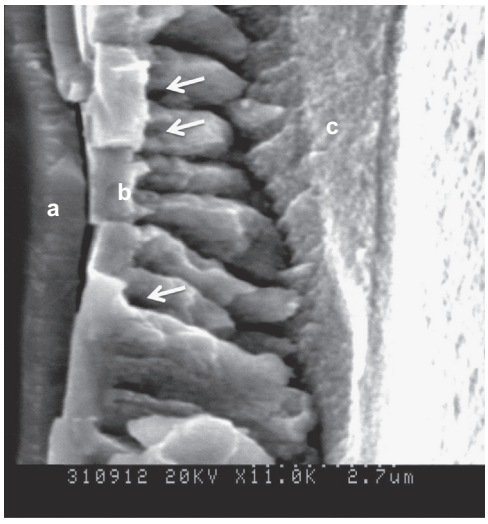

Fig. 3. SEM micrograph corresponding to the fracture of the coated system; (a) DLC coating; (b) CrC layer; (c) electroless NiP. The various dark spots (pointed out by white arrows), correspond to the Ar incorporation in the coating structure.

Thus, as can be observed from Fig. 5, Cr and C will diffuse towards the NiP alloy, whereas Ni and P diffuse towards the PVD coating, hence establishing a definite interface between a newly formed graded layer of CNiPCr, whose thickness is around 4 μm, and the DLC/CrC PVD coating, with a thickness of approximately 2.2 μm.

Another interesting feature is that related to the change of the feeding rate of the carbon carrier gas in the system, marked by the arrow on the plot. This corresponds to the inflexion point of the C concentration curve, which could be related to the thickness of both the CrC graded layer and the DLC coating of 1.26 μm and 0.9 μm, respectively, corroborating thus the information provided by the suppliers [16].

3.2. Nanoindentation results

3.2.1. Description of the hardness results

The value of the intrinsic hardness of the NiP coating in the as-received condition, as well as its elastic modulus were determined from the nanoindentation results and are presented in Fig. 6a and b. It is clearly shown that, for penetration depths above ~100 nm and 400 nm, for hardness and elastic modulus, respectively, both parameters remain quite constant with the increase in h, indicating that the measurement of these properties has not been influenced by the hardness and elastic properties of the aluminium alloy substrate, as a consequence of the large NiP coating thickness.

Fig. 7a illustrates the change in hardness as a function of penetration depth, corresponding to the results of not less than 70 nanoindentation tests conducted on three different samples of the DLC coated system. The data have been described by means of the modified version of the Jönsson–Hogmark (J–H) model [13], as proposed by Iost et al. [14], for the analysis and description of the composite hardness of multilayer coatings. In this way, by means of non-linear regression analysis, it has been possible to determine the different parameters encompassed in the model.

These include the intrinsic hardness of the DLC film (H_{DLC}), the hardness of the CrC intermediate layer (H_{CrC}), the hardness of another intermediate layer that developed during deposition of the DLC film, as a consequence of the interdiffusion of C, Ni, P and Cr (H_{CNiPCr}) and the hardness of the underlying electroless NiP load-support layer (H_{NiP}), which for the range of penetration depths under consideration can be regarded as the "substrate". The results of the model are represented by the mean curve drawn through the experimental data. Thus, the parameters involved in the model were determined employing more than 20 thousand experimental data points. Details of the different relationships, which encompass the modified J–H model are given elsewhere [14].

As can be observed from Fig. 7a, the hardness versus penetration depth data comprises a scatter band, whose width varies as a function of the penetration depth. At the beginning of the indentation tests, the hardness exhibits a wide scatter and it is observed to vary between approximately 5 and 10 GPa.

According to the modified J–H model, as the indenter displacement increases, the mean composite hardness of the multilayer film is determined initially by the DLC intrinsic hardness, which remains approximately constant at a value in the range of 7 GPa, for an indentation depth range of approximately 82 nm. Such an

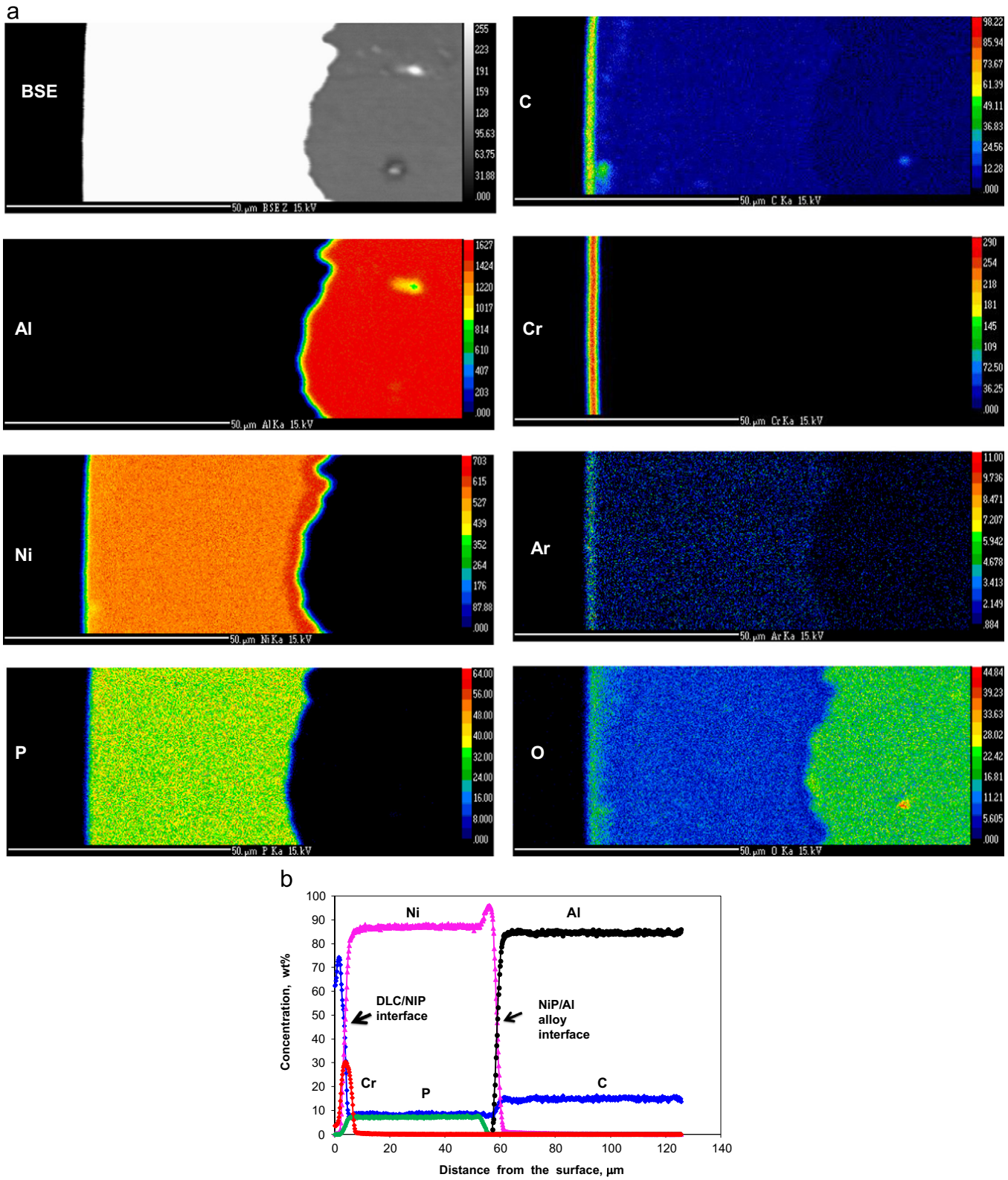

Fig. 4. (a) SEM micrograph and elemental X-ray mapping corresponding to the coated system cross section, carried out by means of electron probe micro analysis (EPMA); (b) Quantitative elemental analysis profile, showing the variation in concentration as a function of distance from the surface.

indentation depth interval is directly proportional to the DLC film thickness. The value of the proportionality constant, C_{DLC}, depends on the behaviour of the film under indentation loading. For a Berkovich indenter and assuming that the DLC film undergoes cracking, $C_{DLC}=0.0915$ [14].

Regarding the transition from the DLC film to the CrC intermediate layer, as the penetration depth continuous to increase about 100 nm, the presence of the CrC intermediate layer, whose intrinsic hardness is significantly higher than that of the DLC film, gives rise to an increase in the mean composite hardness up to a maximum

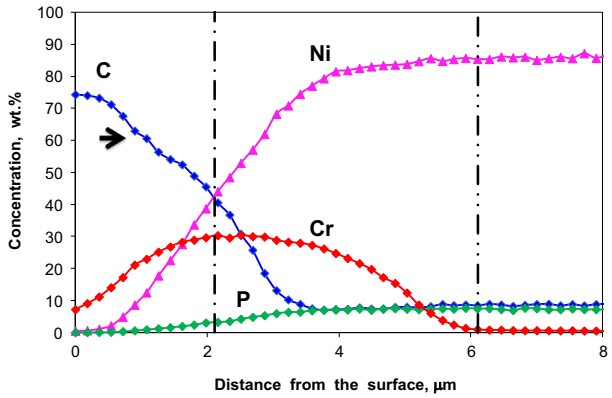

Fig. 5. Quantitative analysis profile, showing the variation of the elemental concentrations of Ni, P, Cr and C that took place at the PVD coating/NiP interface. The change of the feeding rate of the carbon carrier gas in the system is indicated by the arrow on the plot.

Table 1
Variation of Cr, Ni and P composition across each layer thickness.

	Cr (at%)	Ni (at%)	P (at%)
a:C-H	2.0–6.7	0.1–2.4	0.0–0.7
CrC intermediate layer	6.7–12.8	2.4–15.6	0.7–2.2
CNiPCr intermediate layer	12.8–1.1	15.6–59.5	2.2–10.0

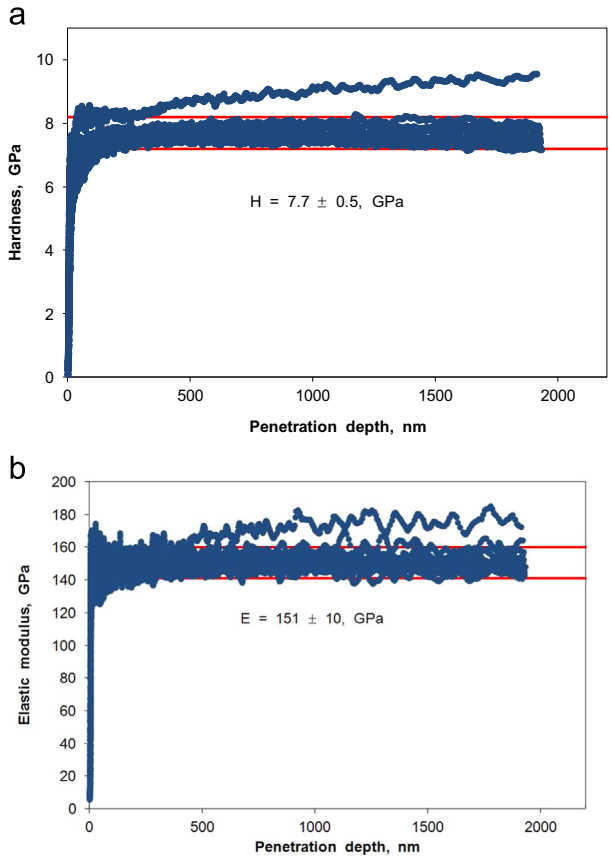

Fig. 6. Results form nanoindentation tests for the as-received NiP coating: (a) variation of the coating hardness with the indenter penetration depth; (b) variation of the elastic modulus with the indenter penetration depth.

value in the range of approximately 14 GPa. Fig. 7a clearly illustrates that such a steady increase in the composite hardness occurs within an indentation depth range of approximately 220 nm, which is also

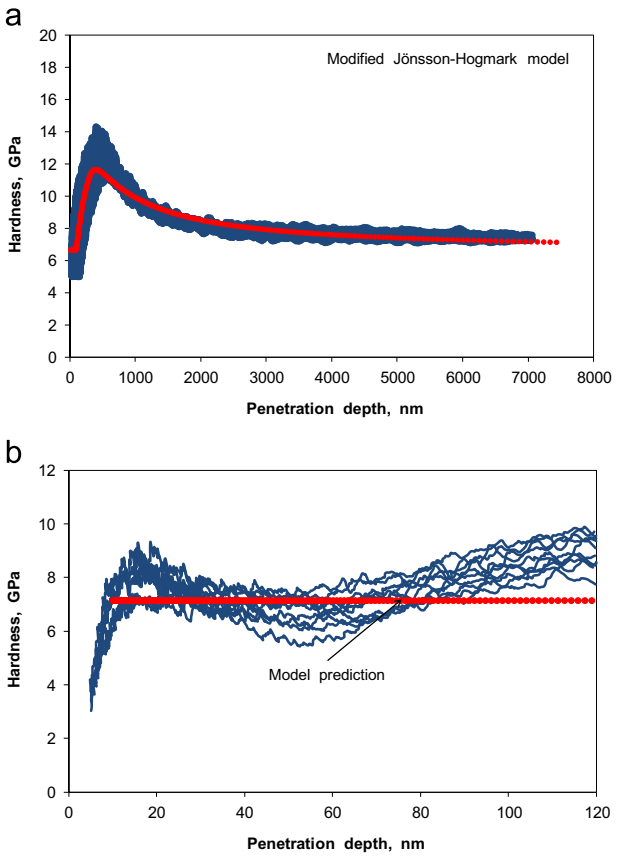

Fig. 7. (a) Change in hardness as a function of penetration depth corresponding to three different samples of the DLC coated system. The data are described by means of the modified of the Jönsson–Hogmark (J–H) model [14]. (b) Hardness versus penetration depth curves employed in the present investigation, just in the interval between 5 and 120 nm.

directly proportional to the CrC film thickness. The value of the proportionality constant depends on the behaviour of this material under indentation loading. By assuming that the CrC film deforms plastically under loading, the proportionality constant between such an indentation depth and the film thickness, $C_{CrC}=0.1746$ [14].

According to Fig. 7a, once the indenter displacement exceeds approximately 700 nm, both the second intermediate layer formed by interdiffusion and the NiP electroless plating start to contribute to the composite hardness, which gives rise to a steady decrease in its value. Fig. 5 indicates that the second intermediate layer formed by interdiffusion has a thickness of approximately 4000 nm. Thus, by considering that such a layer also deforms plastically under indentation loading, the results of the modified JH model point out that its hardness is in the range of 5 GPa, somewhat less than that of the NiP coating.

Thus, modelling was conducted by imposing the condition that the hardness curve becomes asymptotic at 7.1 GPa that, as shown in the forthcoming, represents the intrinsic hardness of the NiP plating after PVD deposition. As indicated above, given the thickness of the NiP plating, for the penetration depth range under investigation, it effectively acts as the "substrate" for the PVD coating.

The hardness value of the DLC film of ~7 GPa determined for the interpretation of the nanoindentation measurements, is somewhat less than the value reported in a previous paper [19], since it represents its intrinsic hardness value and not the combined value corresponding to the DLC and CrC layers.

However, the analysis of the initial part of the hardness curves obtained from the nanoindentation tests allows an explanation of this result. Fig. 7b illustrates a number of hardness versus penetration

depth curves employed in the present investigation, just in the interval between 5 and 120 nm.

The lower limit (5 nm) corresponds to the minimum penetration depth from which it is possible to determine the correct values of the mechanical properties of the fused silica standard commonly used for the calibration of the instrument, which was employed for carrying out the tests. Thus, the calibration of the Berkovich indenter indicated that from penetration depths of ~5 nm a constant value for the elastic modulus of the fused silica standard of ~72 GPa was obtained. As can be observed from these curves, at penetration depths between ~15 and 20 nm, a local hardness maximum is achieved, which ranges between ~7 and 9 GPa. After this maximum, the curves tend to achieve a plateau at a hardness level between ~5 and 8 GPa. Thus, in agreement with these observations, in this range of penetration depths the model predicts a hardness of ~7 GPa, as shown on the plot.

As will be described in the forthcoming, it has been determined that the DLC film has an elastic modulus of approximately 73 GPa, which indicates that the ratio $E/H \approx 10.4$. This parameter is usually employed for determining the degree of plasticity development under the indenter. For hydrogenated carbon films, according to the work conducted by Michler et al. [20], such a ratio is commonly found in the range of approximately 9–10. Therefore, it could be concluded that the estimation of the DLC film hardness is not an artifact of the non-fully developed plasticity. On the contrary, the values in the range of 17–18 GPa, which have been reported for this material could be attributed to the way in which this property is determined, according to the standard procedures usually employed for this purpose.

As an example, the standard ISO14577-4 [21] reports a hardness value of about 18 GPa for a DLC film of approximately 2.5 μm in thickness, determined as the maximum value of the H versus h/t curve, where t represents the thickness of the film. However, in this case the coating is considered as a monolayer film and not as an actual bi-layer coating. If this procedure had been employed in the present analysis, a hardness value of approximately 14 GPa would have been reported, by disregarding the fact that the coating is actually composed of both the DLC film and the CrC intermediate layer, which exhibit different hardness values.

The modified Jönsson–Hogmark model advanced by Iost et al. [14] allows the capture of these important details concerning the determination of the intrinsic hardness values of the different layers, which compose the multi-layer film, an aspect that is not dealt with in the standard indicated above. Moreover, the model predicts the influence of substrate effects only after penetration depths higher than approximately 1000 nm, that is to say, well after the attainment of the maximum exhibited on the H versus h curve of Fig. 7a.

The relatively low hardness value that has been determined in the present investigation for the DLC film could be attributed to a number of reasons. It is well known that the hardness of DLC films deposited by PVD processes depends significantly on the deposition conditions. For example, Michler et al. [20] reported hardness values for amorphous hydrogenated carbon films in the range of approximately 5–23 GPa, depending on the ratio $J/p^{0.6}$ and CH_4 flow. Here, J stands for the current density and p, the pressure. Li et al. [22] also found that the hardness of hydrogenated amorphous carbon (a-C:H) films decreased from approximately 14 GPa to about 9 GPa, when the bias voltage increased from 100 to 500 V. On the other hand, Yamamoto and Matsukado [23] indicated that the hardness of hydrogenated DLC coatings, deposited by means of unbalanced magnetron sputtering, increased linearly from approximately 5 GPa to about 22 GPa when the bias voltage increased from 0 to 100 V.

Porosity could also play an important role in the decrease of the mechanical properties of different materials. As an example, Luo et al. [24] described the change in hardness, H, of 3Y-TZP ceramics as a function of the porosity content, P, by means of a simple parametric relationship of the form:

$$H = H_0 \exp(-\alpha P) \tag{1}$$

where H_0 represents the hardness of the fully dense material and α a constant, whose value was found to be 5.02. Adachi et al. [25] also employed the above equation for the description of the effect of porosity on the hardness of polycrystalline ZrN ceramics and reported that a value of $\alpha = 5.93$ was more appropriate.

Thus, by considering that $H_0 = 14$ GPa for the DLC film under consideration, as indicated by the maximum hardness value on Fig. 7a, the above relationship would predict a porosity for this material in the range of approximately 12–14%, which would also explain the low hardness value observed.

As shown in Fig. 6, for the NiP coating in the as-deposited condition the hardness value corresponding to penetration depths greater than 500 nm was of $\sim 7.7 \pm 0.5$ GPa, which is slightly greater than the hardness value imposed to the modified J–H model of 7.1 GPa. The latter value was obtained experimentally from nanoindentation tests carried out on one of the PVD deposited samples, but on its reverse side, where the DLC coating was not deposited. The results presented in Fig. 8 show that, in this case, a hardness value of 7.1 ± 0.3 GPa was determined.

However, as indicated in Fig. 8b, for the NiP electroless deposit on the reverse side of the DLC coated sample, it was found that the value of the elastic modulus, E, determined was of approximately 140 ± 10 GPa, which is also somewhat less than that corresponding to the NiP in the as-deposited condition.

Thus, these findings would corroborate the microstructural changes that occurred during PVD deposition of the DLC and CrC films on NiP coating.

3.2.2. Analysis of the elastic modulus

Fig. 9 illustrates the change in the elastic modulus of the coating with penetration depth, as reported for more than 70 nanoindentation tests conducted on three different samples. The figure clearly shows that, for the vast majority of the experimental data, for indentation depths greater than approximately 500 nm, the elastic modulus becomes constant at a mean value of about 118 ± 12 GPa.

It is well known that the substrate effects on the elastic modulus can be more pronounced than on hardness since, unlike plastic deformation, the long-range elastic field extends into the substrate, especially when the film thickness is small. Thus, even for very low depths, there is always some elastic deformation of the substrate, which affects the measured modulus at small indentation depths relative to the film thickness, i.e. at $h/t \sim 0.01$ [26]. Therefore, it is difficult to estimate directly the elastic modulus only from indentation data in which case different models could be used to provide this information [27].

In the present work, in order to determine the values of elastic modulus of the DLC/CrC/CNiPCr/NiP layer, a modified form of the model proposed by Perriot and Barthel (P–B) [15] has been employed and the results are presented in Fig. 10.

According to the original version of the P–B model, the composite elastic modulus of a coated system, which encompasses a single coating, is given by simple law of mixtures, of the form:

$$E = E_{Subst.} + a(h)\,(E_{Film} - E_{Subst.}) \tag{2}$$

In the above equation, E represents the composite elastic modulus, E_{Film} and $E_{Subst.}$ the elastic moduli of coating and substrate, respectively and $a(h)$ the volume fraction of coating that contributes to the composite modulus, which is given by the following equation:

$$a(h) = 1 - \frac{1}{1 + (\beta_{PB} t/2.8\,h)^{n_{PB}}} \tag{3}$$

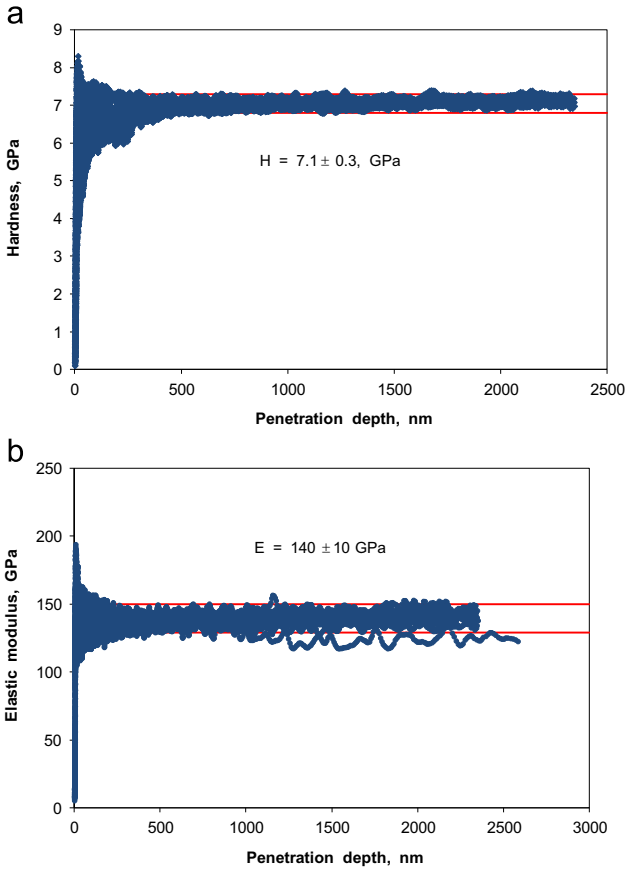

Fig. 8. Nanoindentation results obtained with the NiP electroless deposit, on the reverse side of the DLC coated sample: (a) change in hardness; (b) change in the elastic modulus.

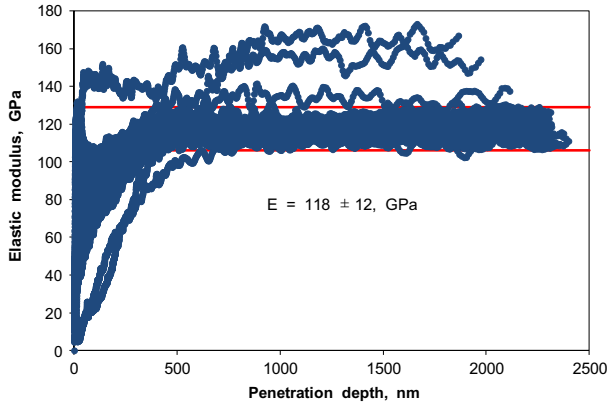

Fig. 9. Change in the elastic modulus of the coating with penetration depth, as reported for more than 70 nanoindentation tests conducted on three different samples.

Here, h represents the penetration depth, whereas β_{PB} and n_{PB} are intrinsic constants characteristic of each layer of the coating.

Thus, Eqs. (2) and (3) were applied in a sequential manner. First, between the DLC film and the CrC intermediate layer, giving rise to a partial description of the elastic modulus, $E(h)_1$. Second, between the CrC and CNiPCr layers, giving rise to a second partial description $E(h)_2$ and finally between the CNiPCr layer and the NiP substrate, giving rise to a third partial description, $E(h)_3$. Subsequently, $E(h)_1$ and $E(h)_2$ were joined by means of a Heaviside equation of the form:

$$F(h,\alpha_H,\beta_H)=\frac{1}{2}\left[1+\tanh\left(\frac{h-\alpha_H}{\beta_H}\right)\right] \quad (4)$$

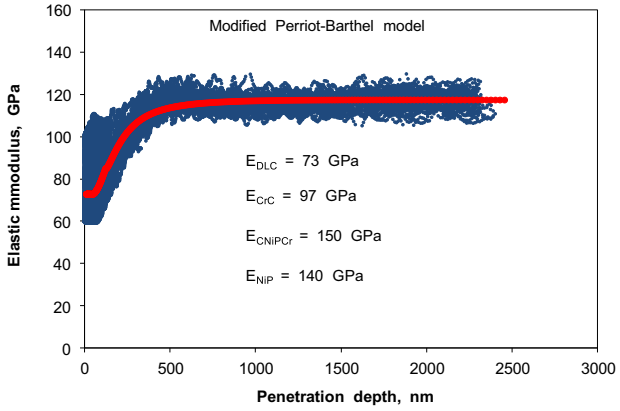

Fig. 10. Variation of the elastic modulus of the different materials involved in the coated system, as a function the of indenter penetration depth. Both the E and H_f values are determined for each layer using a modified form of the model proposed by Perriot and Barthel (P–B) [15].

where α_H and β_H represent constants, which are determined from the experimental data for each pair of layers. This joining operation gave rise to a fourth partial description of modulus, $E(h)_4$, which was joined to $E(h)_3$ by means of a second Heavyside equation, in order to obtained the final description of the experimental data presented in Fig. 10. The values of the elastic modulus of the different materials involved in the coated system are given on the plot.

The value of E found for the CrC intermediate layer agrees with those found by Andersson et al. [28] who carried out deposition by magnetron sputtering of CrC coatings. These authors have reported values for E varying from 100 GPa to 256 GPa as a function of the carbon content in the as-deposited coating, from 25 to 85 at%, respectively. In the present investigation, the change of the carbon content in the CrC graded layer throughout its thickness was determined to be between 80 and 73 at%. However, the experimental values found for the CrC film hardness in the present research do not support the values reported by these authors, since this layer has in its composition the presence small amounts of Ni and P, as a consequence of their diffusion form the NiP plating towards the surface of the coated system.

Similar considerations could be done in relation to the newly formed CNiPCr intermediate graded layer, whose Cr/Ni (wt%) average ratio is about 0.23. Both the E and H_f values determined for this layer (see Fig. 10) are higher than those reported recently from a study conducted by Danısman et al. [29] in order to determine the chromium influence on the mechanical properties of Ni–Cr thin films produced by sputtering for this Cr/Ni ratio. These authors found that when the ratio Cr/Ni is 0.23, the hardness and Young modulus were of 5.5 GPa and 60 GPa, respectively.

Nevertheless, the determined values in the present research correspond to a system that implies the presence of C and P, as consequence of diffusion during processing.

3.3. Scratch results

Fig. 11 shows the variation of load, friction force and acoustic emission signal for the scratch track produced with the displacement of the stylus. This figure also includes the optical micrographs of the track, indicating the possible events that could have taken place.

At the beginning of the scratch, the presence of cracks, which appear at the edge of the track, takes place at 11 N as consequence of the frictional tensile stresses, indicating thus a tensile cracking failure mode. As the load increases, these cracks grow into a semicircular form and become parallel to the trailing edge of the

indenter, being propagated through the coating thickness. Similar coating failures modes were described by Zaidi et al. [30], who studied the adhesion of a PVD DLC deposited on 304 stainless steel.

The first change in the acoustic emission signal occurs at a load of 32.4 N, when the tensile cracking mode of the graded CrC coating starts to be accompanied by conformal cracking, due to a higher compressive stress field found in front of the moving stylus. As the load further increases, spallation takes place at a load of 46.5 N due to through- thickness cracking, typical for an adhesive failure of the coating on a softer substrate. This load is considered as the critical value for coating detachment from which uncovered substrate will be seen regularly and its magnitude indicates, therefore, a good adhesion of this coating onto the NiP plating.

The electron probe micro analyzer (EPMA) micrograph, corresponding to the X-ray mapping of the scratch towards the end of it, shows clearly the presence of the three modes of failures (Fig. 12a–d). These figures also indicate the quantitative evolution of the C, Cr, Ni and P concentrations in the second part of the scratch track starting from the point corresponding to the critical adhesive failure load of 46.5 N, as the scratch normal load increases towards its maximum value of 60 N.

4. Tribological performance of the coated system

4.1. Evaluation of the elastic contact stresses during spherical indentation

The results from the characterization conducted on these systems together with the mechanical and physical properties found in the literature are summarized in Table 2. The elastic properties values could therefore be used for the computation of the change in the von Mises stress with distance from the surface, under the normal load applied during the test. The calculations were conducted on the basis of the Hertzian equations corresponding to the elastic contact between a spherical indenter and a multi-layer coating, taking into consideration the strain compatibility at each interface.

This simplistic approach implied the computation of the principal strains at each interface as a function of the von Mises stresses and elastic constants of the corresponding layer material and the assumption that such strains remained constant across the interface. In this way, both the von Mises stresses and maximum pressure could be re-computed for the subsequent layer. The value of the elastic modulus was interpolated directly from the results shown in Fig. 10.

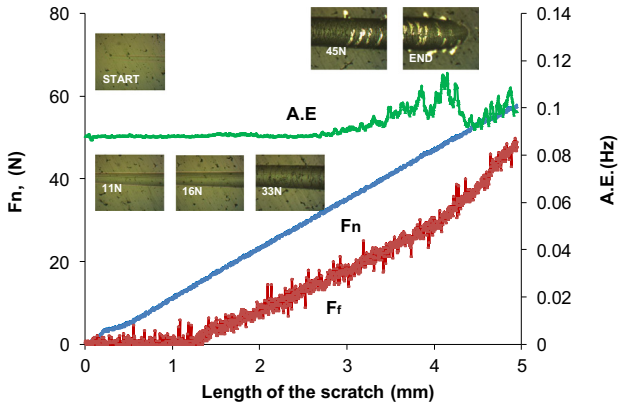

Fig. 11. Variation of load, friction force and acoustic emission signal along the scratch track produced with the displacement of the stylus.

The computational procedure employed, involved the interpolation of the predicted values of the elastic modulus from the modified Perriot–Barthel model (Fig. 10), in order to solve the non-linear equation, which allows the determination of the contact radius as a function of the reduced modulus, load applied and indenter diameter. Also, regarding the computation of the principal stresses and the von Mises stress, the Poisson ratio as a function of distance from the surface, was calculated assuming a Heaviside step function.

The results of these calculations are presented in Fig. 13 for 2 and 5 N applied loads. It can be observed that, under these testing conditions, the system behaves elastically and that plastic deformation of the aluminium alloy substrate does not occur, since the von Mises stress at the NiP-substrate interface is below the yield stress of the alloy, which has a value of approximately 450 MPa.

4.2. Friction coefficients and wear performance

The variations of the friction coefficients with the sliding distance for all the three systems under study at two different normal loads are presented in Fig. 14.

For the aluminium alloy system, it can be observed that, as the wear test is carried out, for a normal load of 2 N (contact pressure=0.57 GPa), the value of the friction coefficient increased with the sliding distance and barely achieved a steady state value of 0.8 at 600 m. However, as the load increases to 5 N (contact pressure=0.78 GPa), the average friction coefficient value for the tribological pair aluminium alloy/alumina counterpart decreased to a value of 0.5 and the steady state was achieved much sooner, at 150 m. This value agrees with that of the friction coefficient reported for an A356 aluminium alloy [33] that has been tested against an alumina ball, with a contact pressure of almost the same magnitude (0.75 GPa) and a sliding velocity of 0.03 m/s.

The same trend was observed for the NiP coating in relation to the influence of the normal load on the friction coefficients values, obtaining an average friction coefficient of 0.5 and 0.4 for a normal load of 2 N and 5 N, respectively.

However, almost no difference was found for the DLC/alumina ball system, since the maximum average friction coefficient for 2 N was of 0.12, whereas for a 5 N normal load it was of 0.1, as expected, since its value was found to drop with the increase in the normal load. A similar friction behaviour was reported by Bull [38] in a previous work. This author indicated that for hydrogenated DLC, the friction coefficient drops during the early stages of the test wear (see Fig. 11). Nevertheless, these values are higher than those reported in the literature for a-C:H coating [39], since during the sliding wear test the amount of the relative humidity was as high as 60%.

The profilometry results allowed the determination of an average cross section area with a scatter, which varies between 7 and 15%. These values are presented in Table 3 together with those for the wear rate, k, for each sample.

As can be observed, a very high wear rate was obtained for the uncoated aluminium alloy due to the high amount of material transfer to the harder ball, as corroborated by the values determined form the 2D profile of the wear track. The values for the friction coefficient and wear rate are of the same order of magnitude as those reported in the literature for a similar tribological pair and normal loads [40].

A considerable reduction of nearly three orders of magnitude in the wear rate value was obtained when the aluminium samples were coated with electroless NiP. The DLC deposition brought about a further reduction in the wear constant value, which was more than one order of magnitude higher than of the NiP

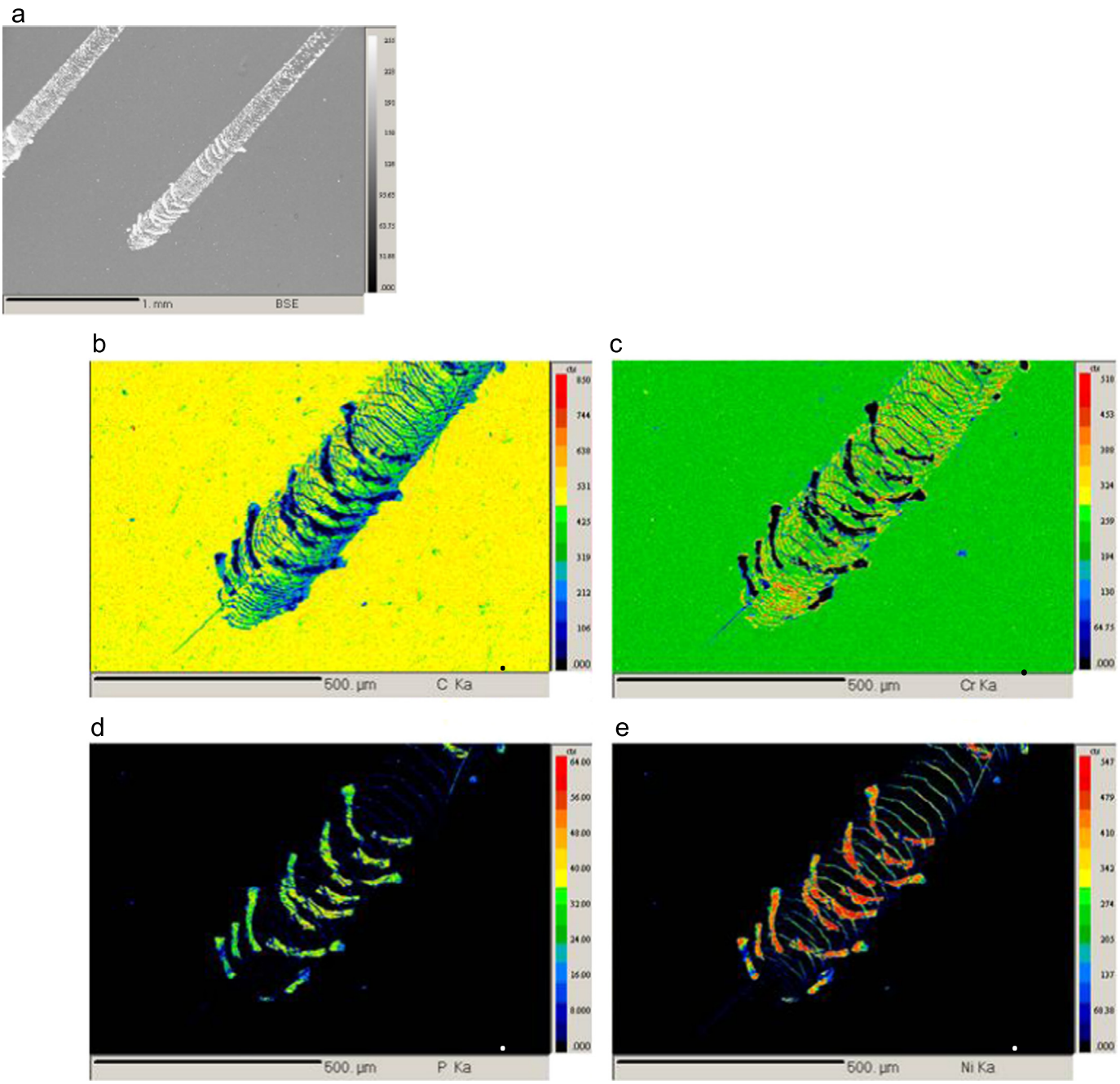

Fig. 12. (a) Electron probe micro analysis (EPMA) micrograph and X-ray mapping of the scratch track starting from the point of the critical adhesive failure load of 46.5 N, indicating the quantitative evolution of: (b) C; (c) Cr; (d) P and (e) Ni concentrations.

Table 2
Mechanical and elastic properties of the coated system.

	Material	Thickness (µm)	Poisson ratio	Hardness (GPa)	Yield stress (GPa)
Indenter	Alumina [31] (E=416 GPa)	infinite	0.231 [31]	15.0 [31]	5.0 [27]
Substrate	2024 Al[a]	infinite	0.33 [32]	0.135 [32]	0.45[a]
Layer 1	NiP	48[a]	0.30 [33]	7.1[a]	2.4 [34]
Layer 2	CNiPCr	4[a]	0.31 [35]	6.4[a]	2.2 [34]
Layer 3	CrC	1.26[a]	0.33 [36]	16.3[a]	5.43 [34]
DLC	a-C:H	0.9[a]	0.30 [37]	7.4[a]	0.37 [37]

[a] Present work.

deposited on top of the aluminium alloy, tested at the same normal load of 2 N. A smaller reduction of approximately 6 times was obtained when the load increased to 5 N (see Table 3). These values, are consistent with those reported in the current literature for the a-C:H films, sliding against various different counterparts [39,41].

4.3. Wear mechanism

Post mortem wear tracks characterization by means of SEM in a S.E. mode allowed the determination of the wear mechanism. The micrographs presented in Fig. 15 for the Al substrate and NiP/Al substrate against the alumina counterpart show the presence of adhesive features and abrasive grooves typical of a contact of this kind of tribological pairs. Such features were more pronounced as both the contact pressure and surface hardness values of the samples decreased. The same characteristics could be seen in the 3D profiles attached to the micrographs. Extensive plastic deformation took place in case of aluminium alloy and the alumina ball displaced a considerable amount of it during sliding.

The adhered alloy was brought back to the sample surface and under the cyclic contact load it would start to work-hardened. Subsequently, a considerable amount of debris would be produced as consequence of different processes that would take place, such as cracking due to fatigue and exfoliation of the metallic substrate material. This debris would be compacted again on the samples surface, generating a new surface, which is harder than that of the original alloy and its hardness value would be proportional to the contact load. Similar phenomena would take place for the NiP/Al alloy/alumina ball, however, to a lesser extent, due to the fact that the hardness of NiP is almost five times higher than that corresponding to the uncoated substrate. Here, the shape of the wear track profiles shows, as in the case of the uncoated aluminium substrate, the existence of an abrasive-adhesive wear mechanism typical of the contact of a hard ball with a soft metallic material [40].

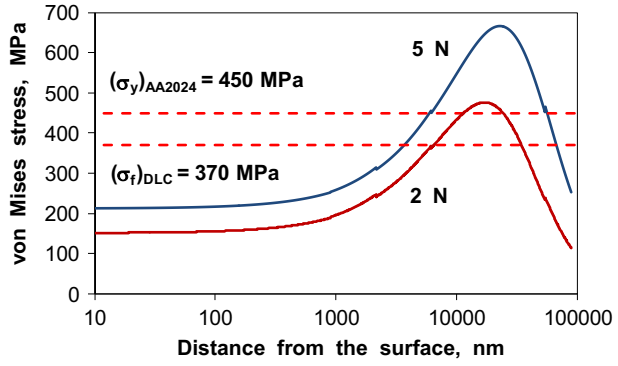

Fig. 13. Change in the von Mises stress with distance from the surface, under the normal load applied during the test of 2 and 5 N, respectively.

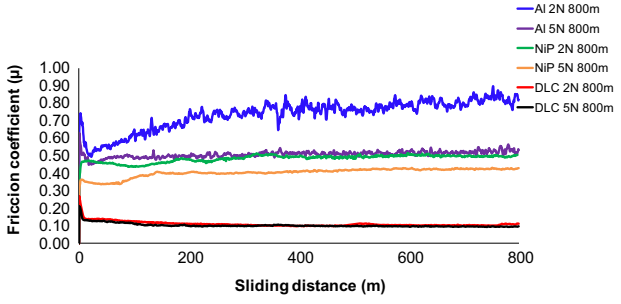

Fig. 14. Variations of the friction coefficients with the sliding distance for the three systems under study at two different normal loads 2 and 5 N, respectively.

For the DLC/CrC/NiP/aluminium alloy the wear mechanism is totally different. The alumina ball produced a slight polishing of the surface for the load applied of 2 N, polishing which is accentuated as the normal load is increased. The shape of the wear track profile indicates debris entrainment, as well as the accumulation of the debris on top of the ball, giving rise to a more pronounced W shape as indicated by Cassara et al. [42]. The mean Hertzian contact pressures for the applied normal loads of 2 N and 5 N are 0.5 and 0.7 GPa, respectively.

Fig. 16 shows the X-ray elemental mapping of the 4 principal elements whose presence and amount was determined by using EPMA, as well as the 3D profiles of the wear track for 2 and 5 N normal, respectively. It could be observed that for both loads, the DLC film is still intact, although very thin, on top of CrC graded intermediate layer and no spallation of the coating during the test took place, indicating its adequate adhesion. The NiP coating was thick enough in order to provide a good support sufficient to avoid plastic deformation of the Al substrate and the premature failure of DLC coating. Moreover, looking at the profilometry traces in 2D for both loads it is observed that the values of the coating penetration depth never is higher than 0.48 μm, indicating that the DLC coating is still present.

Due to the low hardness of the DLC of only 7.4 GPa and the presence of humid air, no wear of the alumina ball took place. The SEM observation of the counterparts has determined the presence of a layer, as a paste, compacted on top of the ball with a higher thickness towards the back side of the contact area, shown in Fig. 17 for a normal load of 5 N load. The semi-quantitative analysis by EDS indicated only the presence of carbon and chromium and no sign of adhesive failure was found, since the presence of NiP was not observed.

Very interesting results that support the above mechanism were presented by Scharf and Singer [43] who studied in situ the wear of a DLC coating with similar elastic modulus, but a higher hardness of 12 GPa. The coating was tested against a sapphire ball (6.35 mm diameter) in air 52% humidity, for a Hertzian mean contact pressure of 0.7 GPa and a sliding velocity of 1 mm/s. These authors have shown that the transfer film thickened as the test was carried out and debris particles became imbedded forming a thick compact layer, which remained stationary in the contact region throughout the test, thus indicating a steady state value for the friction coefficient.

A similar kind of behaviour was reported by Buijnsters et al. [44] for a-C:H films grown by ECR-CVD with different % of hydrogen contents.

It is also interesting to compare the values found in the present research with those reported by Bolleli et al. [9], who carried out tribological tests under similar contact conditions (alumina ball of 6 mm and 5 N normal load) of DLC coatings deposited onto an

Table 3
Results from the evaluation of the wear tracks for all the systems under study.

Tribological pair	Load (N)	Area (m^2)	Volume (m^3)	Wear constant (m^3/N m)
A 2024-T3 aluminium alloy	2	1.8×10^{-7}	34.4×10^{-10}	215×10^{-14}
	5	1.6×10^{-7}	30.5×10^{-10}	197×10^{-14}
NiP/ A 2024-T3 aluminium alloy	2	1.8×10^{-10}	33.1×10^{-13}	207×10^{-17}
	5	2.7×10^{-10}	52.0×10^{-13}	324×10^{-17}
DLC/NiP/A 2024-T3 aluminium alloy	2	0.15×10^{-10}	2.8×10^{-13}	18×10^{-17}
	5	0.5×10^{-10}	9.2×10^{-13}	58×10^{-17}

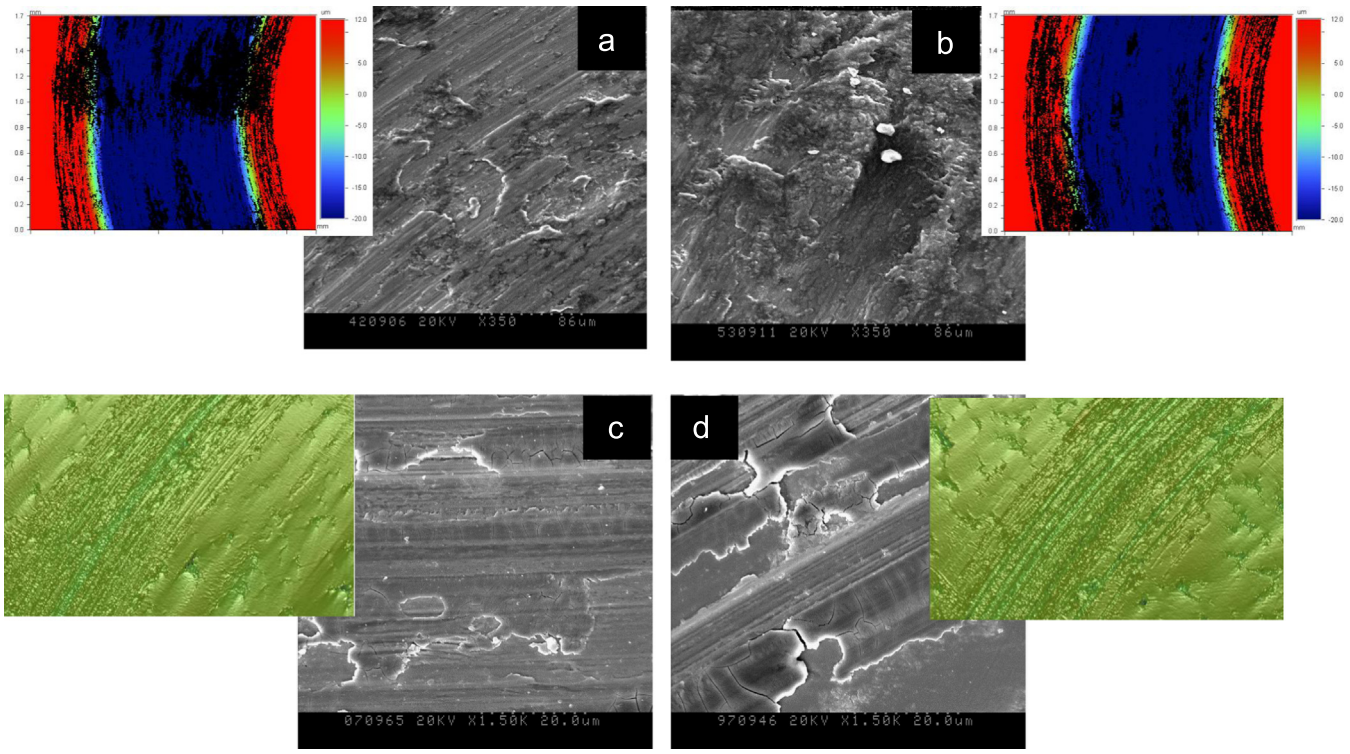

Fig. 15. SEM micrographs and 3D profiles attached to the micrographs of the wear track corresponding to the tribopair: (a) Al substrate/Al_2O_3 at 2 N (b) Al substrate/Al_2O_3 at 5 N; (c) DLC/NiP/Al substrate/Al_2O_3 at 2 N; (d) DLC/NiP/Al substrate/Al_2O_3 at 5 N.

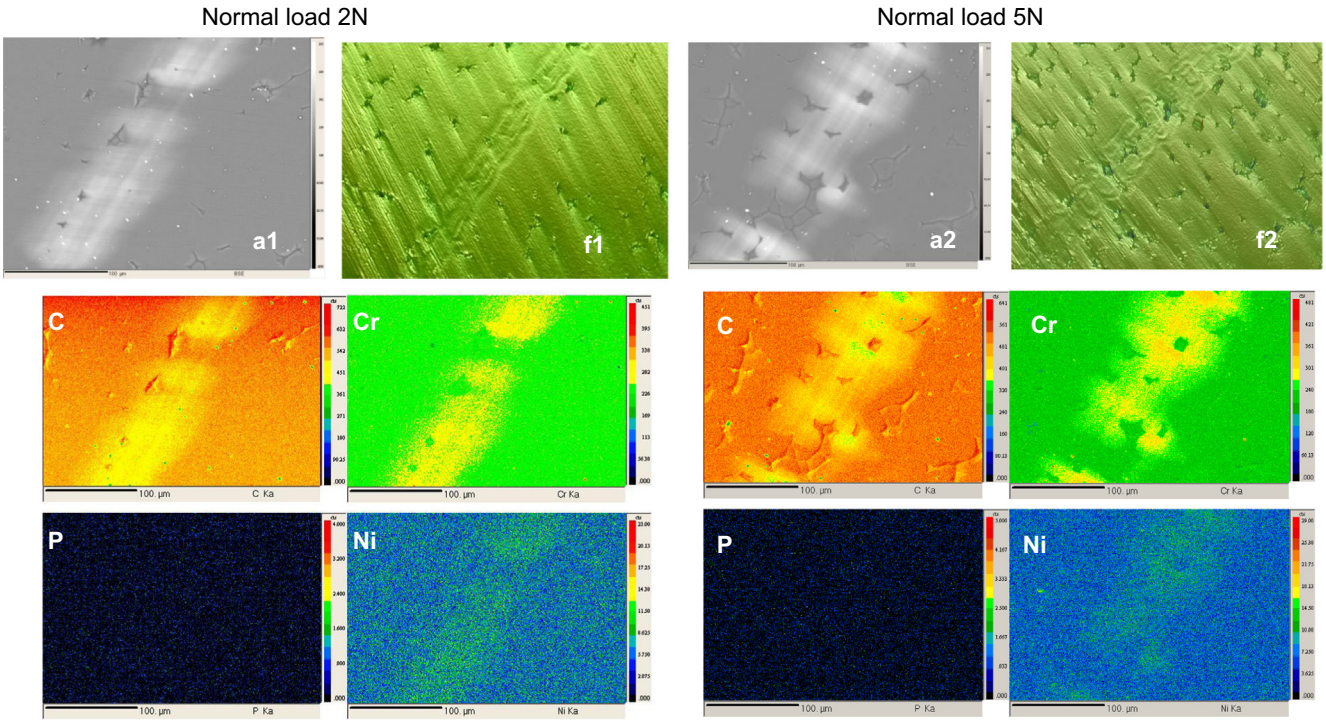

Fig. 16. X-ray elemental mapping of the 4 principal elements using EPMA, as well as the 3D profiles of the wear track for 2 and 5 N normal, respectively.

AA6068-T6 substrate, using a WC-CoCr thermal sprayed coating of 125 μm in thickness, as intermediate layer. The low friction coefficient and the wear response were attributed to the formation of the microcrystalline graphite-like wear debris that could stick to the mating surface. This fact was corroborated by Raman laser spectroscopy. These authors considered that this phenomenon occurred as consequence of large flash temperatures at the contact points between the tribopairs and used the equation proposed by Ashby et al. [45] for evaluating this temperature, which resulted in a value of $\Delta T \sim 300$ °C.

Raman spectroscopy was beyond the scope of the present study. However, since the flash temperature is directly proportional to the sliding velocity and, since in the present research this parameter is almost 6 times smaller (i.e. $\Delta T = 50$ °C), it is thought that this

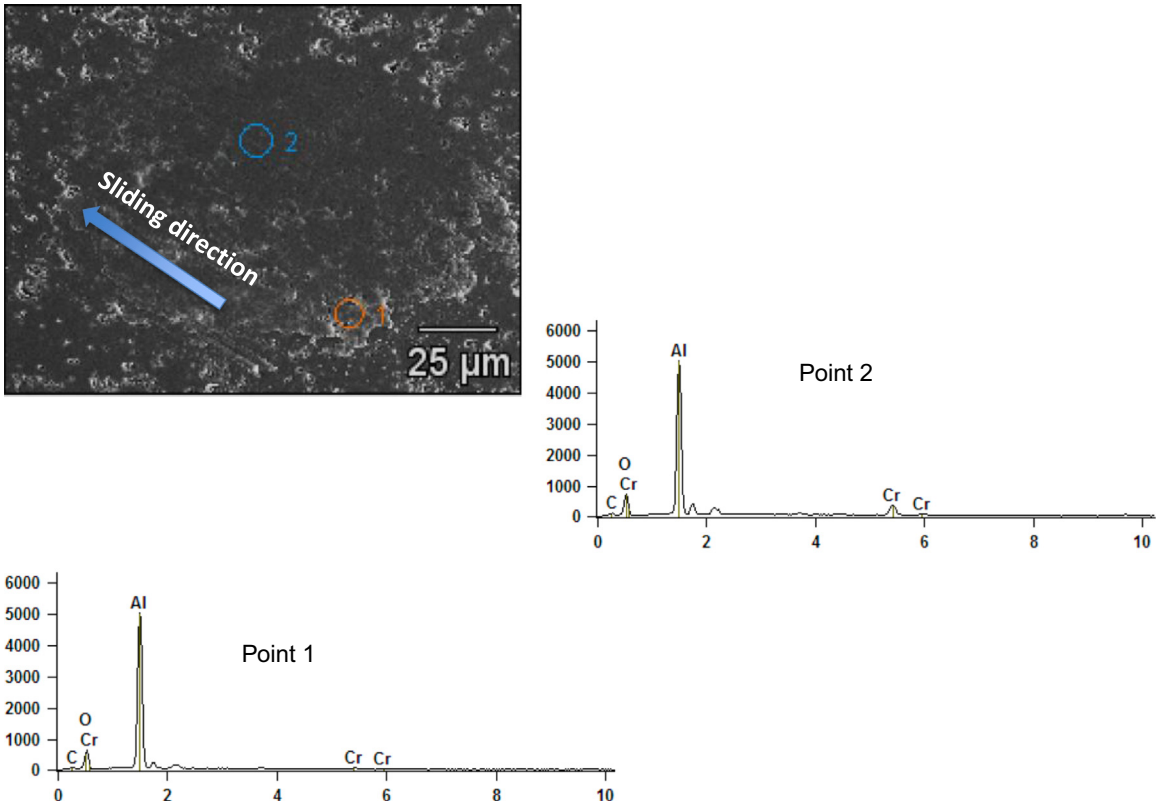

Fig. 17. SEM observation of the counterpart for a normal load of 5 N and semi-quantitative analysis by EDS of the points 1 and 2 indicated on the micrograph.

temperature rise could not probably be sufficient to produce a phase transition process whereby a low shear strength graphite-like layer is formed at the sliding interface. This conclusion is supported by the results reported by Bhushan [46], who studied the influence of sliding velocity and load on the wear of DLC coatings. Moreover, it has also been shown that the relative humidity could considerably reduce the nominal contact temperature and, consequently, promotes a reduced graphitization [5].

5. Conclusions

Tribological sliding tests conducted on an AA2024-T6 aluminium alloy coated with a multilayer DLC/CrC/CNiPCr/NiP coating, indicated that under maximum contact pressures greater than 1 GPa, a wear rate of approximately 6×10^{-16} m^3/m N is obtained, which is one order of magnitude smaller than that of the substrate coated with electroless NiP and almost four order of magnitude smaller than that corresponding to the uncoated aluminium alloy. The presence of this new CNiPCr graded layer indicated above, with a thickness of approximately 4 μm, was determined by means quantitative EPMA analysis carried out on the coated sample cross section. It is believed that such a layer was formed as a consequence of inter-diffusion between the DLC and NiP coatings during deposition. These findings, together with a careful morphological characterization by means of scanning electron microscopy, have allowed the correct interpretation of the indentation results. In this way, the mechanical properties of the DLC/CrC/CNiPCr/NiP coating have been satisfactorily characterized by means of nanoindentation testing techniques. The change in the composite hardness of the coated system with penetration depth has been described by means of the modified form of the Jönsson-Hogmark model advanced by Iost et al. [14]. Thus, the intrinsic hardness of each individual layer has been determined taking into consideration its mechanical behaviour under indentation. On the other hand, it has been possible to describe the change in the elastic modulus with penetration depth by means of a modified form of the model earlier advanced by Perriot–Barthel [15]. The model has been applied by parts between the layers and the global behaviour has been described satisfactorily by joining the individual curves with appropriate Heaviside transfer functions. In this way, it has also been possible to determine the individual elastic modulus of each layer of the coating. The predicted values of the elastic modulus with penetration depth have been subsequently employed in the computation of the change in von Mises stress with distance from the surface by means of the classical Hertzian formulation, which involves the elastic contact of a spherical indenter subjected to a normal load, with a multilayer coating, taking into consideration the compatibility of strains at each interface. The results of such an analysis indicate that the coated system is able to maintain its integrity when contact pressures greater than 1 GPa are applied, without the occurrence of the plastic failure of the aluminium alloy substrate, in agreement with the results of the sliding tests.

Acknowledgements

Professor Staia acknowledges the financial support from of the Scientific and Humanistic Development Council of the Universidad Central de Venezuela (CDCH-UCV) through project AIB-08-8539-2012 and also to Arts et Métiers Paris Tech, (ENSAM Lille), France. Professor Puchi-Cabrera gratefully acknowledges the financial support of the Conseil Régional Nord-Pas de Calais, France, through the International Chair program 2011.

References

[1] Apachitei I, Duszczyk J. Autocatalytic nickel coatings on aluminium with improved abrasive wear resistance. Surf Coat Technol 2000;132:89–98.

[2] Vitry V, Sens A, Kanta AF, Delaunois F. Wear and corrosion resistance of heat treated and as-plated Duplex NiP/NiB coatings on 2024 aluminum alloys. Surf Coat Technol 2012;206:3421–7.
[3] Sudagar J, Venkateswarlu K, Lian J. Dry sliding wear properties of a 7075-T6 aluminum alloy coated with Ni–P (*h*) in different pretreatment conditions. J Mater Eng Perform 2010;19(6):810–8 (August).
[4] Yin Z, Chen F. Effect of nickel immersion pretreatment on the corrosion performance of electroless deposited Ni–P alloys on aluminium. Surf Coat Technol 2013;228:34–40.
[5] Hauert R. An overview on the tribological behavior of diamond-like carbon in technical and medical applications. Tribol Int 2004;37:991–1003.
[6] Spies HJ. Surface engineering of aluminium and titanium alloys: an overview. Surf Eng 2010;26(1–2):126–34.
[7] Xie ZH, Singh R, Bendavid A, Martin PJ, Munroe PR, Hoffman M. Contact damage evolution in a diamond-like carbon (DLC) coating on a stainless steel substrate. Thin Solid Films 2007;515:3196–201.
[8] Biasoli De Melloa JD, Binderb R. A methodology to determine surface durability in multifunctional coatings applied to soft substrates. Tribol Int 2006;39:769–73.
[9] Bolelli G, Bonferroni B, Coletta G, Lusvarghi L, Pitacco F. Wear and corrosion behaviour of HVOF WC–CoCr/CVD DLC hybrid coating systems deposited onto aluminium substrate. Surf Coat Technol 2011;205:4211–20.
[10] Wanstrand O, Larsson M, Kassman-Rudolphi A. Mechanical and tribological properties of vapour deposited low friction coatings on Ni plated substrates. Tribol Int 2000;33:737–42.
[11] Pawlak, W, Kubiak, KJ, Wendler, BG, Mathia, TG, Wear resistant multilayer nanocomposite WC1x/C coating on Ti–6Al–4V titanium alloy, http://dx.doi.org/10.1016/j.triboint.2014.05.030.
[12] Wang L, Wan S, Wang SC, Wood RJK, Xue QJ. Gradient DLC- based nanocomposite coatings as a solution to improve tribological performance of aluminum alloy. Tribol Lett 2010;38:155–60.
[13] Jönsson B, Hogmark S. Hardness measurements of thin films. Thin Solid Films 1984;114:257–69.
[14] Rahmoun K, Iost A, Keryvin V, Guillemot G, Sari NE Chabane. A multilayer model for describing hardness variations of aged porous silicon low-dielectric-constant thin films. Thin Solid Films 2009;518:213–21.
[15] Perriot A, Barthel E. Elastic contact to a coated half-space—effective elastic modulus and real penetration. J Mater Res 2004;19:600–8.
[16] Jarratt M, Stallard J, Renevier NM, Teer DG. An improved diamond-like carbon coating with exceptional wear properties. Diamond Relat Mater 2003;12:1003–7.
[17] Oliver WC, Pharr GM. Measurement of hardness and elastic modulus by instrumented indentation: advances in understanding and refinements to methodology. J Mater Res 2004;19:3–20.
[18] Schonjahn C, Lewis DB, Munz WD, Petrov I. Substrate ion etching in combined steered Cathodic arc–UMB deposition system: effects on interface architecture, adhesion and tool performance. Surf Eng 2000;16(2):176–80.
[19] Puchi-Cabrera ES, Staia MH, Ochoa-Pérez EA, Teer DG, Santana-Méndez YY, La Barbera-Sosa JG, et al. Fatigue behaviour of a 316L stainless steel coated with a DLC film deposited by PVD magnetron sputtering ion plating. Mater Sci Eng, A 2010;527:498–508.
[20] Michler T, Grischke M, Traus I, Bewilogua K, Dimigen H. Mechanical properties of DLC films prepared by bipolar pulsed DC PACVD. Diamond Relat Mater 1998;7:1333–7.
[21] Norme Européenne NF EN 14577-4, Matériaux Métalliques: Essai de pénétration instrumenté pour la détermination de la dureté et des paramètres de matériaux. Partie 4: Méthode d'essai pour les revêtements métalliques et non métalliques; 2007.
[22] Li HX, Xu T, Chen JM, Zhou HD, Liu HW. The effect of applied dc bias voltage on the properties of a-C:H films prepared in a dual dc–rf plasma system. Appl Surf Sci 2004;227:364–72.
[23] Yamamoto K, Matsukado K. Effect of hydrogenated DLC coating hardness on the tribological properties under water lubrication. Tribol Int 2006;39:1609–14.
[24] Luo J, Stevens R. Porosity-dependence of elastic moduli and hardness of 3Y-TZP ceramics. Ceram Int 1999;25:281–6.
[25] Adachi J, Kurosaki K, Uno M, Yamanaka S. Porosity influence on the mechanical properties of polycrystalline zirconium nitride ceramics. J Nucl Mater 2006;358:106–10.
[26] Borrero-López O, Hoffman M, Bendavid A, Martin PlJ. Substrate effects on the mechanical properties and contact damage of diamond-like carbon thin films. Diamond Relat Mater 2010;19:1273–80.
[27] Saha R, Nix WD. Effects of the substrate on the determination of thin film mechanical properties by nanoindentation. Acta Mater 2002;50:23–38.
[28] Andersson M, Högström J, Urbonaite S, Furlan A, Nyholm L, Jansson U. Deposition and characterization of magnetron sputtered amorphous CrC films. Vacuum 2012;86:1408–16.
[29] Danısman M, Cansever N. Effect of Cr content on mechanical and electrical properties of Ni–Cr thin film. J Alloys Compd 2010;493:649–53.
[30] Zaidi H, Djamai A, Chin KJ, Mathia T. Characterisation of DLC coating adherence by scratch testing. Tribol Int 2006;39:124–8.
[31] Munro RG. Evaluated material properties for a sintered alpha-Al_2O_3. J Am Ceram Soc 1997;80:)1919–28.
[32] ⟨asm.matweb.com/search/SpecificMaterial.asp?bassnum=MA2024T3⟩.
[33] Yoshida A, Fujii M. Influence of soft surface modification on rolling contact fatigue strength of machine element. Tribol Int 2002;35:837–47.
[34] Tabor D. In: Blau PJ, Lawn BR, editors. Microindentation techniques in materials science and engineering, ASTM STP 889. Philadelphia, PA: American Society for Testing and Materials; 1986. p. 5–24.
[35] Faraoun H, Aourag H, Esling C, Seichepine JL, Coddet C. Elastic properties of binary NiAl, NiCr and AlCr and ternary Ni_2AlCr alloys from molecular dynamic and Abinitio simulation. Comput Mater Sci 2005;33:184–91.
[36] Lia Y, Gao Y, Xiao B, Min T, Yang Y, Ma S, et al. The electronic, mechanical properties and theoretical hardness of chromium carbides by first-principles calculations. J Alloys Compd 2011;509:5242–9.
[37] Staia MH, Puchi-Cabrera ES, Iost A, Carrasquero E, Santana Mendez YY, La Barbera Sosa JG, et al. Sliding wear of a-C:H coatings against alumina in corrosive media. Diamond Relat Mater 2013;38:139–47.
[38] Bull SJ. Tribology of carbon coatings: DLC, diamond and beyond. Diamond Relat Mater 1995;4:827–36.
[39] Donnet C, Fontaine J, Grill A, Le Mogne T. The role of hydrogen on the friction mechanism of diamond-like carbon films. Tribol Lett 2000;9(3-4):137–42.
[40] Cree D, Pugh M. Dry wear and friction properties of an A356/SiC foam interpenetrating phase composite. Wear 2011;272:88–96.
[41] Field SK, Jarratt M, Teer DG. Tribological properties of graphite-like and diamond-like carbon coatings. Tribol Int 2004;37:949–56.
[42] Cassara G, Avelar-Batista Wilson JC, Banfielda S, Housden J, Matthews A, Leyland A. A study of the reciprocating-sliding wear performance of plasma surface treated titanium alloy. Wear 2010;269:60–70.
[43] Scharf TW, Singer IL. Role of third bodies in friction behavior of diamond-like nanocomposite coatings studied by in situ tribometry. Tribol Trans 2002;45(3):363–71.
[44] Buijnsters JG, Camero M, Vázquez L, Agulló-Rueda F, Gago R, Jiménez I, et al. Tribological study of hydrogenated amorphous carbon films with tailored microstructure and composition produced by bias-enhanced plasma chemical vapour deposition. Diamond Relat Mater 2010;19:1093–102.
[45] Ashby MF, Abulawi J, Kong HS. Temperature maps for frictional heating in dry sliding. Tribol Trans 1991;34:577–87.
[46] Nanotribology, nanomechanics and materials characterization. In: Bhushan, editor. Nanotechnology. 2nd ed. Springer Science; 2007. p. 819–20.